Addition of Chitosan to Silicate Cross-Linked PEO for Tuning Osteoblast Cell Adhesion and Mineralization

Akhilesh K. Gaharwar, Patrick J. Schexnailder, Qu Jin, Chia-Jung Wu, and Gudrun Schmidt*

Purdue University, Weldon School of Biomedical Engineering, West Lafayette, Indiana 47907, United States

ABSTRACT The addition of chitosan to silicate (Laponite) cross-linked poly(ethylene oxide) (PEO) is used for tuning nanocomposite material properties and tailoring cellular adhesion and bioactivity. By combining the characteristics of chitosan (which promotes cell adhesion and growth, antimicrobial) with properties of PEO (prevents protein and cell adhesion) and those of Laponite (bioactive), the resulting material properties can be used to tune cellular adhesion and control biomineralization. Here, we present the hydration, dissolution, degradation, and mechanical properties of multiphase bio-nanocomposites and relate these to the cell growth of MC3T3-E1 mouse preosteoblast cells. We find that the structural integrity of these bio-nanocomposites is improved by the addition of chitosan, but the release of entrapped proteins is suppressed. Overall, this study shows how chitosan can be used to tune properties in Laponite cross-linked PEO for creating bioactive scaffolds to be considered for bone repair.

KEYWORDS: Bio-Nanocomposites • Silicate • Laponite • Chitosan • PEO • Cell Adhesion • Mineralization

1. INTRODUCTION

Chitosan-based materials and their applications have generated considerable attention in the biomedical and biotechnologically important fields (1−3). The antibacterial nature, biocompatibility, and biodegradability combined with some of the polymeric properties of chitosan can be used to design advanced polymer bio-nanocomposite materials. Chitosan is a linear and high molecular weight polysaccharide composed of D-glucosamine and N-acetyl-D-glucosamine residues, which are linked together by β-(1,4)-glycosidic bonds (1−3). The N-acetyl-D-glucosamine residues suggest bioactivity due to their similarity with glycosaminoglycans (GAG), and the cationic charges of chitosan interact electrostatically with anionic charged molecules such as GAGs, which are themselves linked to growth factors (3, 4). By varying the molecular weight and deacetylation degree, wound healing properties of chitosan can be enhanced (5). Chitosan favorably interacts with cells, and cellular lysozyme degrades chitosan in vivo (6). Moreover, chitosan has been found to promote adhesion and proliferation of osteoblasts (7, 8) as well as stimulate osteogenesis via osteoblast differentiation and the release of angiogenic factors in vitro (9).

Difficulties persisting with using chitosan-based biomaterials however include weak mechanical properties and poor processing abilities. Some of these processing and mechanical deficiencies can be overcome by blending with other natural or synthetic polymers such as chitin/chitosan or alginate. Such blending has been successfully used for treating healing-impaired wounds (10). Other studies have shown that chitosan blended with synthetic polymers leads to superior materials that may promote nerve regeneration (11); induce bone growth (12); and enhance ligament restoration (13), skin regeneration (14, 15), and cartilage formation (16, 17). Overall, the mechanical properties of biological tissues remain difficult to replicate with polymers or polymer blends alone (18, 19) despite much success in controlling their chemical and biological properties individually. Therefore, other strategies have to be found that mimic the complexity of natural, often multiphase, materials.

We have developed a series of cell adhesive bio-nanocomposite hydrogels from synthetic PEO that is cross-linked by silicate nanoparticles (Laponite) and chitosan (20). The mechanical properties of these hydrogels and materials made from hydrogels are dominated by the silicate cross-linked PEO whose synthesis does not pose any problems with reproducibility. We found that the addition of small amounts of chitosan to PEO-Laponite hydrogels enhanced fibroblast cell adhesion and added advantageous properties of chitosan without hampering mechanical strength (20). Preliminary cell growth studies indicated that fibroblasts readily grow on these materials and attach to the silicate cross-linked PEO surfaces more readily than to the pure PEO surfaces (21, 22).

Motivated by our preliminary studies, in this contribution, we investigate the effect of chitosan on the physical, chemical, and biological properties of silicate cross-linked PEO bio-nanocomposites. Silicate biomaterials, such as bioglasses, have already been observed to promote bone formation (23−25). While pure silicates do not stand up to the mechanical properties required by bone, the combination of polymer and silicates offers versatility, especially in engineering mechanically strong bioactive matrixes for bone

* Corresponding author. Tel.: +1 765 496 1427. Fax: +1 765 496 1912. E-mail: gudrun@purdue.edu.

Received for review July 12, 2010 and accepted October 1, 2010

DOI: 10.1021/am100609t

repair (26−28). We show how the addition of chitosan influences structural stability and mechanical properties and model drug release and degradation/dissolution properties of the bio-nanocomposites. We present data on osteoblast cell growth and show how chitosan and silicate containing polymer bio-nanocomposites promote the formation of a mineralized extracellular matrix, thus offering new strategies for creating bioactive scaffolds.

2. MATERIALS AND METHODS

Materials. Laponite RD (LRD), a synthetic layered silicate consisting of nanoparticles (diameter, 25−30 nm; thickness, 1 nm), was obtained from Southern Clay. Poly(ethylene oxide) (PEO) with a M_w of 1000 kg/mol and a molecular mass distribution of ca. 1.5 was purchased from Polysciences Inc. A low molecular weight chitosan (20−200 cps) obtained from crab shells with a 75−85% deacetylation degree was purchased from Sigma-Aldrich.

Preparation of Bio-Nanocomposite Films. A 2.5 wt % chitosan acidic solution was prepared by adding 2.5 g of chitosan to 100 g of 0.1 M hydrochloric acid (HCl). PEO and silicate (LRD) were dissolved in different amounts of deionized water and were mixed to form gels. Clear chitosan solutions in HCl and 0.099 M NaOH solutions were added to the PEO/silicate gel drop by drop while stirring vigorously. A series of transparent to translucent hydrogels was obtained. Confocal microscopy and small angle X-ray scattering (SAXS) determined the presence of distribution of aggregates within the nanocomposite hydrogel network. The number of the micrometer-scale aggregates (a few micrometers in size) visible by confocal microscopy was strongly related to the concentration of chitosan. The aggregates were distributed uniformly within the network. Preliminary SAXS data suggested the presence of additional aggregates in the range of 900−2500 nm (20). Without further formulation and addition of other salts to the hydrogels, there is a maximum concentration of chitosan achievable above which the PEO−Laponite−chitosan gels will phase-separate (Figure 1). Multilayer films were made from gels using a solvent evaporation method (20, 21, 29). The films were dried and stored overnight under vacuum conditions before use. The compositions of the final dried films made from hydrogels are listed in Figure 1.

Optical Microscopy. The formation of aggregates was monitored by optical microscopy (Olympus BX51, Melville, New York). To evaluate the degree of aggregation as a function of chitosan concentration, the raw optical images were converted into black and white images using an intensity threshold. Then, the cumulative area fractions were obtained from the processed images using ImageJ software (National Institute of Health (NIH)).

Hydration Kinetics. Hydration properties were measured using a gravimetric methods where nanocomposite samples of different compositions (1.5-cm-diameter circular disks) were allowed to hydrate in phosphate-buffered saline (PBS) at 25 °C. Samples were periodically weighted until a saturation plateau was reached. The hydration degree was defined as the weight ratio of the net liquid uptake to the dried sample using the following equation:

$$\text{hydration degree} = \frac{(M_{wet} - M_{init})}{M_{init}} \times 100$$

where M_{init} represents the initial dry weight and M_{wet} represents the wet weight of the nanocomposite films.

In Vitro Degradation/Dissolution Properties. Static and dynamic degradation/dissolution tests were performed in triplicate on the nanocomposite films. In the static tests, media were not changed over the course of the experiment. In dynamic tests, all media were replaced every 24 h. The nanocomposite films were immersed into 20 mL of PBS at 37 °C for static degradation tests and 2 mL of PBS or a PBS/lysozyme solution (1.5 mg/mL) for dynamic tests. The percentage of mass lost was determined after 1, 4, 7, 14, 21, and 28 days using following equation:

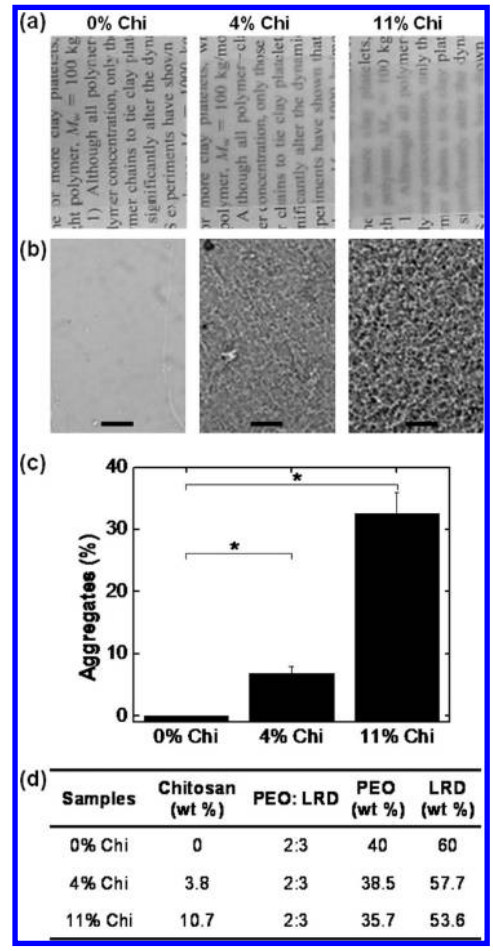

Samples	Chitosan (wt %)	PEO: LRD	PEO (wt %)	LRD (wt %)
0% Chi	0	2:3	40	60
4% Chi	3.8	2:3	38.5	57.7
11% Chi	10.7	2:3	35.7	53.6

FIGURE 1. Effect of chitosan on optical properties of nanocomposites. (a) Optical transmittance of nanocomposite films decrease with an increase in chitosan concentration. (b) The number and size of aggregates increases with an increase in chitosan concentration. The transparency of films is directly proportional to the size and amount of aggregates (scale bar represents 50 micrometers). (c) Amount of aggregates, as a function of chitosan concentration, is calculated from the optical images ($n = 3$). Statistical analysis of these data reveals a significant difference in the amount of aggregates between the samples (indicated by an asterisk). The microscopic images were converted into a black and white image using a threshold value, and then the percent area was calculated using ImageJ (NIH). (d) Composition of nanocomposites films are listed in weight percent.

$$\%\ \text{mass lost} = \frac{(M_o - M_d)}{M_o} \times 100$$

M_o represents the original mass of the dried film, and M_d represents the dried mass after the test. The in vitro degradation of chitosan was determined by comparing the degradation/dissolution degree of the nanocomposite films in PBS and a PBS/lysozyme solution (1.5 mg/mL) for 28 days under dynamic conditions.

Protein Release Kinetics. To determine the effect of chitosan on protein release, albumin was entrapped within nanocom-

posite hydrogels using solvent mixing, and nanocomposite films were fabricated from the well mixed hydrogel. Protein release was determined by soaking the nanocomposite films (cut in 1.5 cm diameter circular discs) in 1 mL of PBS at 25 °C and in 24-well plates. At specific time points, a 1 mL aliquot was withdrawn from each well and 1 mL of PBS was added. The albumin concentration in the aliquot was determined using the commassie blue assay. The absorbance at 595 nm was recorded with a SpectraMax M5 microplate reader. All release studies were carried out in triplicate. The accumulated albumin in solution was calculated and plotted versus time to determine the protein release kinetics. The results are presented in terms of cumulative release as a function of time:

$$\text{cumulative amount released} = \left(\sum_{t=0}^{t=t} {}^{M_t}/_{M_0}\right) \times 100$$

where M_t is the cumulative amount of released albumin from the nanocomposite at time t and M_o is the initial amount of loaded albumin.

Mechanical Properties. Mechanical properties of fully hydrated nanocomposite films (in PBS at 37 °C) were measured using an Ares strain-controlled rheometer and an AR 2000 stress-controlled rheometer (TA Instruments Ltd.; $n = 3$). All experiments were performed using a 20 mm parallel plate geometry and a gap of 100 micrometers. A solvent trap was used to minimize drying of the hydrated film. Oscillatory stress sweep experiments of the nanocomposite films were performed at a frequency = 1 Hz to determine the storage modulus G' and the loss modulus G''. Stress relaxation of the nanocomposite films was determined by subjecting the samples to 1% shear strain and then monitoring the shear stress for 300 s.

Cell Adhesion, Spreading Proliferation, and Viability. MC3T3-E1 subclone 4 mouse preosteblast cells were purchased from the American Type Culture Collection (ATCC). Cells were grown in Dulbecco's Modified Eagle's Medium (DMEM) supplemented with 10% fetal bovine serum (FBS), 100 U/mL penicillin, and 100 μg/mL streptomycin. Films were cut into 1.5-cm-diameter circular discs, briefly submersed in 70% ethyl alcohol and allowed to dry under sterile conditions for all experiments. For growth curve and viability experiments, films and control wells were seeded at 7500 cells/cm^2 in ultra-low attachment 24-well plates (Corning), and the medium was changed every other day. Cell number was quantified by incubation with the CellTiter 96 AQueous One Solution Cell Proliferation Assay (Promega) following the manufacturer's protocol. Cell viability was determined using the Multitox-Fluor Multiplex Cytotoxicity Assay kit (Promega). For adhesion and spreading experiments, cells were seeded at 15 000 cells/cm^2. After 3 h, cells were fixed using 3.7% formaldehyde solution. The cytoskeleton of cells was labeled with Alexa Fluor 488 phalloidin fluorescent dye (Invitrogen). Fluorescent images were taken with an Olympus FV1000 confocal microscope with an excitation wavelength of 488 nm. Representative images are shown.

Cell Differentiation Studies. The effect of chitosan on cell differentiation was determined by seeding preosteoblast cells on nanocomposite films in an osteogenic medium, consisting of DMEM, 10% FBS, 0.283 μM ascorbic acid phosphate, 10 mM β-glycerophosphate, 100 U/mL penicillin, and 100 mg/mL streptomycin. Alkaline phosphatase (ALP) activity was used as an early marker for osteoblast differentiation. The nanocomposite films seeded with preosteoblast cells were cultured for 3, 5, 7, 14, and 21 days ($n = 3$), the cell-grown nanocomposite films were washed twice with PBS, followed by adding a cell lysis buffer containing 0.2% Triton X-100 for 45 min. Samples were collected and stored at −20 °C. ALP activity was measured using the QuantiChrom Alkaline Phosphatase Assay Kit (DALP-250) according to manufacturer's instructions (BioAssay Systems). The absorbance was recorded at 405 nm at time zero ($t = 0$), and again after every 1 min for 10 min ($n = 4$) on a plate reader. Enzyme activity was expressed as μmol/(L · min). Calcium phosphate (PO_4^{3-}) present in a mineralized extra cellular matrix was detected using a standard von Kossa staining. Nanocomposite films grown with preosteoblast cells in osteogenic media for 28 days were fixed with a 3.7% formaldehyde solution. Samples were rinsed with 1 mL of deionized water five times. Afterwards, samples were incubated with 1 mL of 5% silver nitrate solution and were exposed to UV radiation for 1 h.

Statistical Analysis. Data are presented as mean ± standard error of the mean values. Statistical analysis was performed using Minitab (version 16, Minitab Inc., USA) to determine statistical differences. Statistical comparisons were performed with one-way analysis of variance (ANOVA) for an average of 3−5 replicates. After ANOVA was performed on the data set, Tukey's method was used to test all pair-wise mean comparisons. Statistical significance for all tests was set at a P value < 0.05.

3. RESULTS AND DISCUSSIONS

The addition of chitosan to silicate (Laponite) cross-linked poly(ethylene oxide) (PEO) is used for tuning nanocomposite material properties and tailoring cellular adhesion and bioactivity. By combining the advantageous characteristics of chitosan (charged, promotes cell adhesion and growth, antimicrobial) with those of the PEO polymer (hydrophilic, prevents protein and cell adhesion) and those of a layered silicate (positively and negatively charged, potentially bioactive), the resulting material properties can be used to tailor cellular adhesion and control biomineralization.

First, the hydration, dissolution, degradation, and mechanical properties of multiphase bio-nanocomposites are presented. The structural integrity of these materials is found to be improved by the addition of chitosan, but the release of entrapped protein is suppressed. The physical properties can be related to osteoblast cell growth to show how the chitosan and silicate containing PEOs promote the formation of a biomineralized extracellular matrix. Overall, this study shows how chitosan can be used to tune properties in Laponite cross-linked PEO for developing new strategies for creating bioactive scaffolds.

3.1. Effect of Chitosan on Aggregation Properties.

On the macroscopic scale, dried nanocomposite films made from PEO-Laponite hydrogels are transparent to the eye. Transparency can be used here to determine the amount and size of micrometer-sized aggregates. The addition of chitosan affects visual transparency and the optical transmittance of the nanocomposite films. Compared to bionanocomposite hydrogels described before (20), the dried films made from these gels are more transparent than the hydrogels themselves. Figure 1a qualitatively shows how transparency decreases with increased chitosan concentration. The decrease in transparency is mainly attributed to the formation of multiphase aggregates, which are composed of silicate, PEO, and chitosan (Figures 1b,c). A degree of aggregation was determined from optical microscopy using ImageJ (NIH). A series of representative microscopy images shown in Figure 1b indicate a trend in structural changes and a uniform distribution of aggregates within the

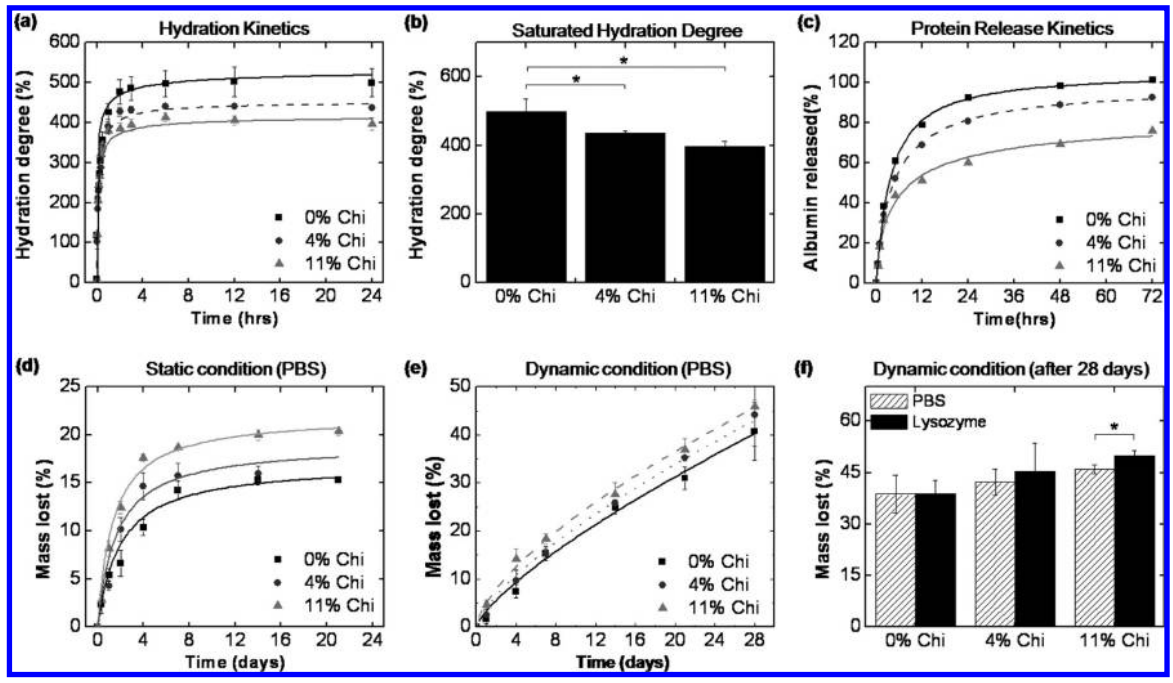

FIGURE 2. Influence of chitosan on structural integrity of nanocomposites and release kinetic of entrapped protein. (a) All the nanocomposite films hydrate quickly in PBS and reach equilibrium within 6 h. (b) The saturation hydration degrees of the films are statistically different (indicated by an asterisk) and decrease with an increase in chitosan concentration. The addition of chitosan results in the formation of a denser network that enhances structural integrity ($n = 3$). (c) The addition of chitosan retards the release of entrapped protein (albumin) due to the formation of a denser network. Degradation/dissolution of films was determined under (d) static and (e) dynamic conditions. Under static conditions, the solution was not changed during the course of the experiment, while under dynamic conditions, the solution was changed every other day. The static test resulted in linear mass loss during the initial days and reached a plateau after around 8 days. The dynamic test resulted in linear mass loss of the film. Under both conditions, mass loss of the films is dependent on chitosan concentration. In both static and dynamic tests, films with chitosan kept their structural integrity, while the films without chitosan fell to pieces ($n = 3$). (f) To monitor in vitro chitosan degradation, films were subjected to PBS and lysozyme solution (1.5 mg/mL) for 28 days under dynamic conditions (solution was changed every alternate day). Nanocomposites containing 11 % chitosan show significant enzymatic degradation of chitosan (indicated by an asterisk).

individual samples. Statistical analysis of these data reveals a significant difference in the amount of aggregates between the samples. Figure 1c summarizes the aggregation in percentage as a function of chitosan concentration.

In our previous work on bio-nanocomposite hydrogels, we found that aggregates first form during the hydrogel preparation process (20). Chitosan is positively charged below a pH of ~6.5 and can strongly interact with the negatively charged silicate surfaces, whereas PEO contains neutral moieties. The positively charged chitosan can also intercalate between the Laponite nanoplatelets via an ion-exchange reaction (30, 31). The presence of protonated amino groups on the chitosan chains results in the formation of strong electrostatic interactions with silicate nanoplatelets by replacing surface cations (31, 32). Thus, the aggregates observed in optical microscopy can be attributed to the formation of ionic complexes formed between chitosan and the PEO covered silicate.

3.2. Chitosan Improves Structural Integrity. The structural stability of bio-nanocomposites under physiological conditions is required for a vast range of drug delivery and tissue engineering applications. Since structural integrity is closely related to the hydration properties, the hydration of a potential biomaterial influences its surface characteristics, diffusion properties, degradation rate, and mechanical strength. The bio-nanocomposites investigated here contain hydrophilic PEO and Laponite nanoparticles; thus a significant change in physical and chemical properties is expected upon exposure of the material to an aqueous environment.

The effect of chitosan on the hydration properties of the PEO-Laponite nanocomposites was monitored by determining the percent hydration degree of the films in PBS at 37 °C. Figure 2a shows that all of the nanocomposite films hydrate quickly and reach an equilibrium hydration degree within ca. 6 h. The saturated hydration degrees for all of the nanocomposite films are significantly different from each other (Figure 2b). The equilibrium hydration decreases with increased chitosan concentration, suggesting that interactions of the chitosan with Laponite and PEO must be present; thus the chitosan is more than just filler. Both PEO and silicate nanoparticles are hydrophilic in nature and thus will increase the hydration. Chitosan is soluble only in acidic solution (pH < 6.5) but not in water at pH = 7; thus an increase in hydration is not expected. The decrease in the overall saturation hydration degree can be attributed to the strong ionic interactions between charged chitosan and charged silicate nanoparticles via the formation of ionic complexes. These interactions strengthen the polymer network by acting as additional cross-linkers which reduce the overall hydration and swelling of the nanocomposites.

Our results can be compared to those from Zheng et al., who found that the addition of chitosan to gelatin/montmorillonite nanocomposites decreased the saturated hydration degree (33). In a similar way, Zivanovic et al. demonstrated

that the addition of chitosan to PEO resulted in reduced solubility and enhanced structural stability (34). Another study by Kabiri et al. reported that the addition of chitosan-intercalated montmorillonite (MMT) to poly(2-acrylamido-2-methylpropane sulfonic acid) hydrogels resulted in a lower swelling capacity and increased thermal stability (35). This group observed that the formation of chitosan−MMT complexes within the hydrogels resulted in delayed swelling at higher temperatures. Overall, these data show that ionic complexes between chitosan and silicate nanoparticles (clays) improve structural stability by reinforcing the polymer nanocomposite network.

In our case, the hydration properties of the nanocomposite network directly influence solute and solvent transport mechanics. The initial hydration data of the nanocomposite samples were fitted to $M_t/M_{eq} = kt^n$ (where M_t = mass of water uptake at time t M_{eq} = equilibrium water uptake, k = characteristic swelling constant, and n = characteristic exponent describing the mode of water transport) to determine the solute transport mechanism (36, 37). The value of n for all of the nanocomposites was less than 0.5 (data not shown), indicating Fickian diffusion (diffusion governed by a concentration gradient). Similar trends were reported by Guilherme et al. on montmorillonite-crosslinked maltodextrin-co-dimethylacrylamide nanocomposites (38). This group attributed the swelling mechanism of nanocomposite hydrogels to a diffusion process that resulted from the physical−chemical interactions between the solvent and matrix.

3.3. Chitosan Retards Release of Entrapped Protein. The effect of chitosan concentration on the release kinetics of an entrapped model macromolecular drug (albumin) is summarized in Figure 2c. All of the nanocomposite samples exhibit a burst release of the entrapped albumin within the first 4 h. The release rate is lower with a higher chitosan concentration and became more sustained after 12 h. The addition of chitosan retards the release of entrapped albumin, and the burst release is suppressed at higher chitosan concentrations. This result is consistent with the hydration kinetics data (Figure 2a). The nanocomposite network and presence of ionic complexes strongly influence the initial burst release as a denser network, containing higher amounts of chitosan cross linkers, and result in a slower release of the protein.

Sustained release of an entrapped drug was also reported by Depan et al., who studied the interactions between chitosan-g-lactic acid, MMT silicate nanoparticles, and Ibuprofen (39). The main differences between the MMT polymer nanocomposites and the Laponite polymer nanocomposites studied here is that MMT will not degrade, while Laponite has the potential to degrade under certain conditions (40).

3.4. In Vitro Degradation of Chitosan within the Nanocomposite Network. Chitosan favorably interacts with the cells, and cellular enzymes degrade chitosan in vivo by lysozymes (6). Thus, immersing the bio-nanocomposite in a solution of PBS and lysozyme should lead to faster degradation of the chitosan within the PEO−Laponite matrix. The effect of chitosan on the degradation and dissolution properties of the bio-nanocomposites was determined by monitoring the weight loss of the films under "static" and "dynamic" conditions. Under static conditions, the medium was not changed during the course of the experiment; under dynamic conditions, the medium was changed every day. The resulting degradation/dissolution profiles of the bio-nanocomposite films are shown in Figure 2d,e. Under "static" conditions (Figure 2d), the calculated mass loss reached a plateau after ca. 8 days. The mass loss of samples measured after 21 days is directly dependent on the chitosan concentration. Data fitting indicated that the degradation/dissolution rates followed first-order kinetics. Under dynamic conditions (Figure 2e), a steady weight loss was observed while the trend was near linear. To summarize, under both static and dynamic conditions, the nanocomposite films containing chitosan showed higher dissolution/degradation rates compared to films without chitosan. Moreover, the nanocomposites containing higher amounts of chitosan retained their structural integrity after 21 days, whereas nanocomposites without chitosan slowly disintegrated.

To distinguish between the dissolution of the PEO−Laponite network and the chitosan degradation, all samples were subjected to a PBS and to a PBS−lysozyme (1.5 mg/mL) solution for 28 days at 37 °C (Figure 2f). The lysozyme concentration used in the medium was similar to that found in human serum (41). The degradation/dissolution rates of the samples with and without chitosan were measured in both mediums (solvent changed every other day), and the results are summarized in Figure 2f.

The data suggest that the total mass loss increases when the medium is changed from PBS to PBS/lysozyme solution. Statistical analysis of these data reveals a significant mass loss in the nanocomposite films containing 11% chitosan when the medium was changed from PBS to PBS/lysozyme. The increase in chitosan degradation by lysozyme was estimated by comparing the materials' mass loss in PBS with the materials' mass loss in PBS−lysozyme. Lyzozyme is expected to affect only the chitosan degradation; thus no considerable differences in mass loss were expected and observed in PEO−Laponite films without chitosan (Figure 2f). Regarding the chitosan degradation within an organic−inorganic nanocomposite, our results can be compared to those of Zhuang et al., who investigated gelatin−montmorillonite−chitosan nanocomposites in lysozyme solution (42), and to work by Niu et al., who investigated chitosan/hydroxyapatite/collagen/poly(L-lactic acid) nanocomposites (43).

3.5. Chitosan Enhances Mechanical Properties. Consideration of mechanical properties under physiological conditions is essential to the design of bio-nanocomposite materials for biomedical use. Since appropriate mechanical strength is important to the design of bioactive surfaces and interfaces that support cell growth, it is imperative to understand the polymer−nanoparticle interactions that are responsible for inducing and maintaining mechanical strength.

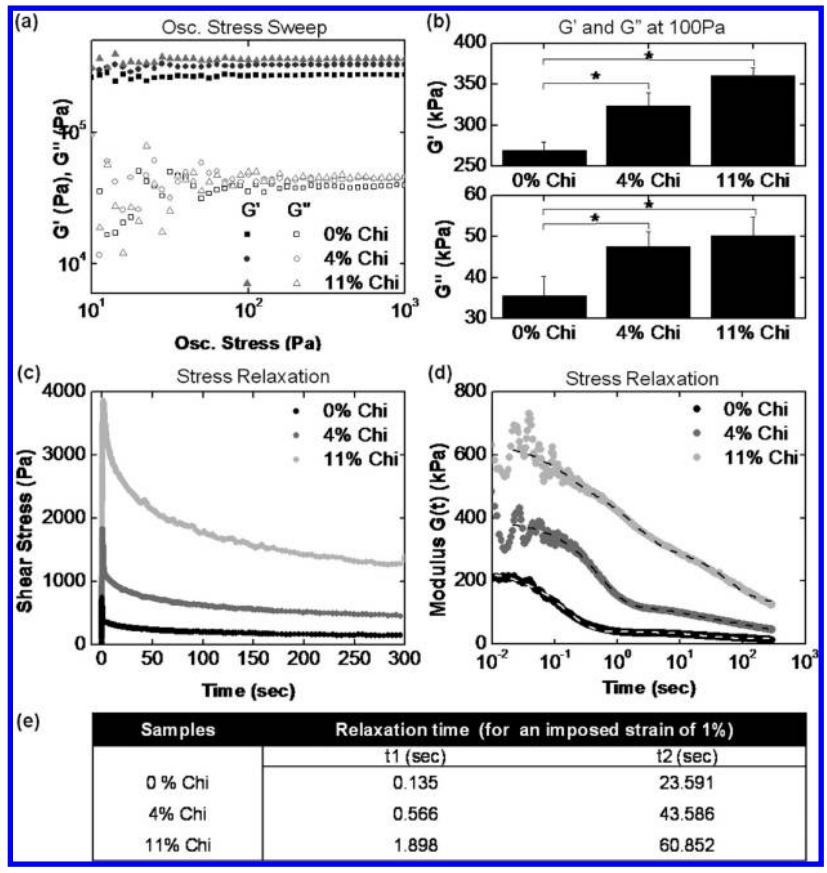

(e)

Samples	Relaxation time (for an imposed strain of 1%)	
	t1 (sec)	t2 (sec)
0 % Chi	0.135	23.591
4% Chi	0.566	43.586
11% Chi	1.898	60.852

FIGURE 3. Improvement of the mechanical strength of nanocomposite due to chitosan. (a) The effect of chitosan on the mechanical properties of nanocomposites was determined using an oscillatory stress sweep at 37 °C and a frequency of 1 Hz. All of the nanocomposites show linear viscoelastic behavior between 10 and 1000 Pa. The elastic modulus (G') is always greater thnn the viscous modulus (G'') for all of the nanocomposite samples. (b) Both storage and loss modulus increase with an increase in chitosan concentration. A significant difference between the moduli of samples containing different amounts of chitosan was observed (indicated by an asterisk). (c) Chitosan significantly influences the stress relaxation behavior of the nanocomposite network. An initial strain of 1% was applied to the sample, and shear stress was monitored for 300 seconds. Chitosan increases initial stress, equilibrium stress, and relaxation time. (d) Stress relaxation moduli as a function of time. (e) Summary of relaxation times obtained after data fitting with $G(x) = \sum G(k) \exp(-x/t)$.

The effect of chitosan on the mechanical properties of fully hydrated bio-nanocomposite films was evaluated by oscillatory shear experiments at 37 °C. First, oscillatory stress sweep experiments were performed where a progressively increasing shear stress was applied to the sample, and the dynamic moduli (elastic G' and viscous G'') were measured. Figure 3a indicates a broad linear viscoelastic region with the elastic modulus (G') being always larger than the viscous modulus (G''). The influence of chitosan concentration on the moduli of the swollen films is shown in Figure 3a,b. Both elastic and viscous moduli increase with an increase in chitosan concentration. A significant difference between the moduli of samples containing different amounts of chitosan was observed. This can be mainly attributed to the uniform dispersion of chitosan−silicate polyelectrolyte complexes within the nanocomposite network (20).

Stress relaxation experiments were performed in order to characterize the response of the fully hydrated PEO−Laponite−chitosan network to a step change in strain. The stress relaxation behavior of the swollen hydrogel like nanocomposite films was determined by subjecting the samples to 1 % strain and then monitoring shear stress as a function of time. Figure 3c shows qualitatively the effect of chitosan on the initial stress, equilibrium stress, and overall relaxation behavior of the nanocomposites network. With an increase in chitosan concentration, increases in initial and equilibrium stresses were observed. Nanocomposites without chitosan recover more quickly towards an equilibrium stress. Figure 3d shows the dependence of stress relaxation moduli ($G(x)$) as a function of time. The moduli decrease with an increase in time, indicating dissipation of stress within the nanocomposite network. The curves suggest the presence of several relaxation times, and the results from data fitting are summarized in Figure 3e. The experimental data were fitted using

$$G(x) = \sum G(k) \exp(-x/t)$$

which assumes a series of relaxation times (t) and weighted constants $G(k)$ (44). Relaxation occurs at both short times and long times and depends on the chitosan concentration. With increasing chitosan concentration, the short relaxation mode observed for PEO−LRD at $t_1 = 0.1$ s increases to 0.6 s and to 1.9 s (Figure 3e). Since this mode at $t_1 = 0.1$ s is present for the pure PEO−LRD sample, it must be related to the stress relaxation of the PEO−LRD network, which includes polymer relaxation or Laponite relaxation within

the network or both. Chitosan thus hinders the fast relaxation of the PEO−LRD network structures. A second relaxation mode observed first at $t_2 = 24$ s (for PEO−LRD) also increases with chitosan concentration. This mode could be related to the relaxation of PEO−LRD aggregates with the network. Again, the presence of chitosan slows down the relaxation of aggregates, as can be seen in the changing trend of t_2.

Overall, these results suggest that the addition of chitosan significantly influences the stress relaxation behavior of the nanocomposite networks, and more work needs to be done to determine the exact origins of the relaxation modes. Recovery and stress relaxation of a physically cross-linked network is important in determining self-healing properties of these materials, which is of significant biomedical interest.

3.6. Cell Growth and Adhesion Studies. The cell adhesion, spreading, and cytoskeleton organization are important parameters in evaluating the cellular compatibility and suitability of biomaterials for a required application. PEO-based materials have already been used to control cellular adhesion. The antibacterial nature, biocompatibility, and biodegradability of chitosan combined with some of the polymeric properties of PEO can be used to design advanced polymer bio-nanocomposite materials (3, 4). Chitosan promotes adhesion and proliferation of osteoblasts (7, 8) and stimulates osteogenesis in vitro (9). Our own preliminary data have shown that fibroblast cell adhesion and spreading can be induced by incorporating silicate nanoparticles in a PEO matrix (21, 22). Here, we show how chitosan allows for tuning the adhesion properties of osteoblast cells to the hydrated PEO−Laponite−chitosan surfaces.

The effect of chitosan on cell adhesion and spreading was determined by seeding the nanocomposites with preosteoblast cells. Figure 4a shows a series of confocal images of films seeded with osteoblast cells after 3 h. Cells readily attached to the nanocomposite surfaces and exhibited protruding arms. With an increase in chitosan concentration, an increase in cell adhesion and spreading was observed (Figure 4b,c). The nanocomposite films containing 11% chitosan show significantly higher cell spreading when compared to 0% chitosan samples and the positive control (TCPS). An increase in chitosan also results in the complex organization of actin filaments within the attached osteoblast cells (Figure 4a). Similar work by Cai et al. showed that a higher number of osteoblast cells adhered to chitosan-modified poly(D,L-lactic acid) films when compared to pure PLA films and that actin stress fibers could be seen on cells, which indicates mature cell matrix adhesion complexes (45). It is recognized that such complex organization of actin filaments is required for initial attachment and subsequent proliferation of osteoblasts on biomaterials (46). A recent study suggests that complex interplay between the cell cytoskeleton, mechanical forces, and biochemical signaling networks are responsible for cell cycle progression and cell fate (including switching between growth, differentiation, and apoptosis) (46, 47).

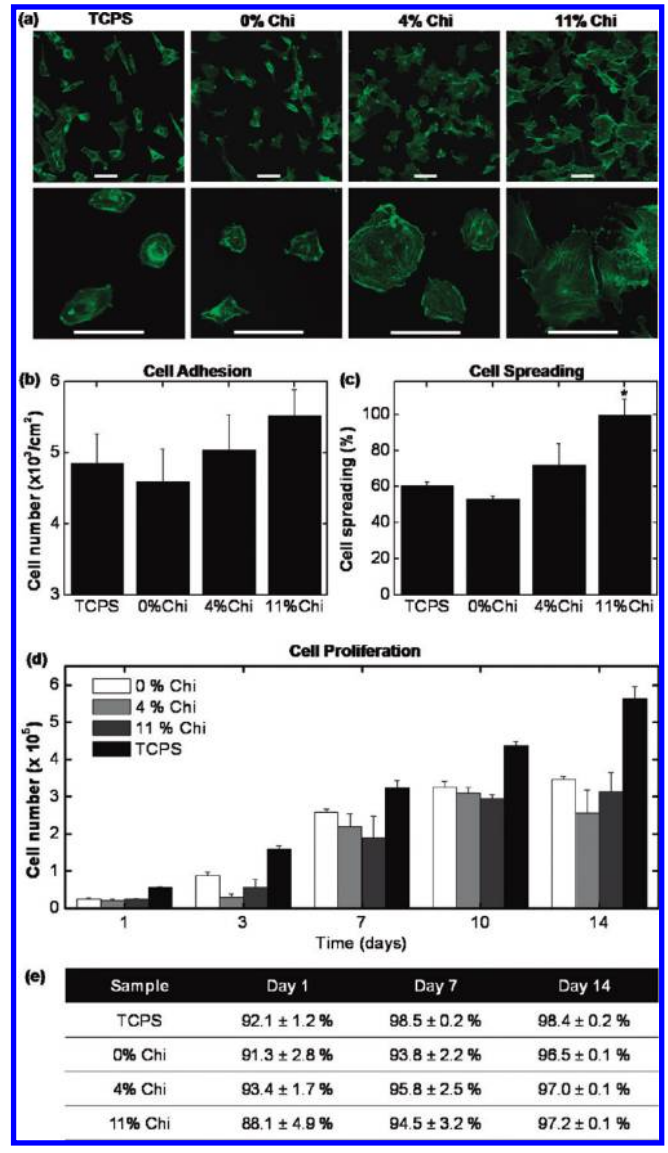

Sample	Day 1	Day 7	Day 14
TCPS	92.1 ± 1.2 %	98.5 ± 0.2 %	98.4 ± 0.2 %
0% Chi	91.3 ± 2.8 %	93.8 ± 2.2 %	96.5 ± 0.1 %
4% Chi	93.4 ± 1.7 %	95.8 ± 2.5 %	97.0 ± 0.1 %
11% Chi	88.1 ± 4.9 %	94.5 ± 3.2 %	97.2 ± 0.1 %

FIGURE 4. Effect of chitosan on adhesion, proliferation, and viability of MC3T3-E1 subclone 4 mouse preosteoblast cells. (a) Cells readily attach to all of the nanocomposites surfaces and exhibit protruding arms due to focal adhesion. The addition of chitosan results in enhanced (b) cell adhesion and (c) spreading on the nanocomposite surface as quantified using ImageJ (NIH). (Scale bar = 50 micrometers.) Nanocomposites containing 11% chitosan have significantly higher cell spreading compared to nanocomposites containing 0% chitosan and positive control (TCPS). (d) All of the nanocomposites support cell proliferation, and no significant difference was observed due to the addition of chitosan. (e) The viability of cells remains high throughout the experiment, and no significant difference in viability was observed due to the addition of chitosan.

The successful formation of functional tissues on a scaffold requires a high degree of proliferation of cells, as the proliferation degree determines the rate of extracellular matrix formation. Figure 4d summarizes the growth characteristic of preosteoblast cells on PEO−Laponite bio-nanocomposites containing different amounts of chitosan. Cells readily grow and proliferate on the nanocomposite surfaces. No considerable differences in cell numbers were observed due to addition of chitosan. The number of cells on TCPS (TCPS = tissue culture polystyrene) at days 10 and 14 are significantly higher compared to all of the other nanocomposites compositions. Similar results were observed using

fibroblast cell lines where cells growing on nanocomposite surfaces did not reach confluency in the plateau phase (22). The cell numbers reached in the plateau phase of the cell growth curves were not a result of contact inhibition between cells, but growth inhibition was found to be dependent on the number and distribution of "cell repellant" PEO and "cell adhesive" silicate regions on the nanocomposite films (22). The viability of cells as determined by a live/dead assay was similar throughout the experimental period (Figure 4e). This indicates that chitosan-containing bio-nanocomposites are nontoxic (in vitro) and that they support cell growth.

3.7. Chitosan Enhances ALP Activity and Differentiation of Osteoblast Cells. After determining how chitosan influences adhesion, spreading, and proliferation of preosteoblast cells on the nanocomposites surfaces, the differentiation of these cells into osteoblast cells was investigated. MC3T3-E1 subclone 4 mouse preosteblast cells can be differentiated by adding ascorbic acid and β-glycerophosphate to the culture media (48, 49). Alkaline phosphatase (ALP) activity was used as an early marker for the osteoblast phenotype. The ALP activity of preosteoblast cells seeded on the nanocomposites containing different amounts of chitosan is shown in Figure 5a. The samples without chitosan display peak ALP activity on day 7, which remains constant on day 14 and day 21. With the addition of 4% chitosan, an increase in ALP activity was observed. Statistical analysis of data indicated that ALP activity of cells seeded on nanocomposites containing 11% chitosan was higher compared to the control (0% chitosan) on days 14 and 21. Moreover, in samples containing 11% chitosan, a progressive increase in ALP activity was observed up to 21 days.

In addition to investigating ALP activity, von Kossa staining was used to visualize the extent of phosphate in the mineralized matrix produced by osteoblast cells after 28 days of culture (Figure 5b). All of the nanocomposite films stained positive for calcium phosphate and displayed a significantly higher mineralized matrix compared to the positive control (TCPS). A chitosan-concentration-dependent response in the amount of mineralized phosphate was observed. The nanocomposites containing 4% and 11% chitosan show significantly higher amounts of mineralized matrix compared to the nanocomposites without chitosan and the positive control (TCPS). When the chitosan concentration increased, e.g., from 0% to 11%, a ca. >40% increase in mineralized ECM was measured. These trends were observed by many research groups on biomaterials containing chitosan. For example, Moreau and Xu reported an increase in ALP activity due to the addition of chitosan in an injectable calcium phosphate–chitosan composite (50). Coutinho et al. reported that the addition of chitosan to poly(butylene succinate) resulted in enhanced protein adsorption on the materials' surface (51), and the expression of a biomarker (ALP activity) indicated the influence of chitosan in differentiation of preosteobalst cells. Similarly, Cai et al. demonstrated that chitosan can be used as a bioactive moiety for enhancing osteoblast proliferation and

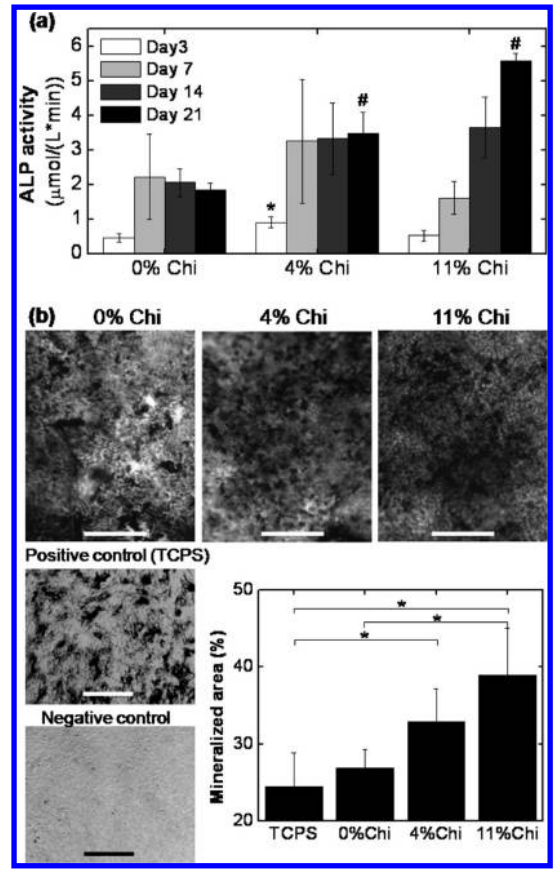

FIGURE 5. Enhancement of alkaline phosphatase (ALP) activity of preosteoblast cells and promotion of the formation of the mineralized extracellular matrix due to chitosan. (a) ALP is an early phase differentiation marker for preosteoblast cells. ALP activity was found to reach a plateau after 7 days in films containing 0 and 4% chitosan. Nanocomposite films containing 11% chitosan show a steady increase in ALP activity until 21 days. A significant increase in ALP activity on day 3 (indicated by asterisk) and day 21 (indicated by hatch) was observed due to the addition of chitosan. (b) When seeded in osteogenic media for 28 days, preosteoblast cells produced a mineralized matrix as determined by dark regions after von Kossa staining. Nanocomposites containing chitosan show significantly enhanced mineralization when compared to the positive control (TCPS; as indicated by an asterisk), suggesting that chitosan influences differentiation of preosteoblast cells positively. Scale bar represent 50 micrometers. Tissue culture polystyrene serves as a positive control.

ALP activity via a surface modification process (45). The increase in ALP activity was associated with the progressive differentiation of preosteoblast cells (52, 53). In another example, Weir and Xu reported that chitosan induces differentiation of preosteoblast cells without affecting proliferation and viability of the cells (54). Finally, a study using polycaprolactone–chitosan scaffolds for bone tissue engineering reported on how the increase in ALP activity, deposition of calcium, and elevated expression of osteopontin were related to chitosan (55). These many results from the literature are in accordance with those presented in this study, indicating that chitosan plays an important role in the differentiation of preosteoblast cells.

4. CONCLUSIONS

We conclude that chitosan-containing silicate cross-linked PEO bio-nanocomposites exhibit unique chemical, physical,

and biological properties due to the complex interactions between the individual components as well as the interactions between the material and cells. Chitosan was found to improve structural integrity of the PEO—Laponite bio-nanocomposite and suppress macromolecular drug release. Moreover, chitosan as well as the silicate influence osteoblast cell spreading and cytoskeleton organization. Increased alkaline phosphatase (ALP) activity was found, and formation of a mineralized extracellular matrix was enhanced by the addition of chitosan, confirming that chitosan influences the differentiation of preosteoblast cells. Overall, this study shows how chitosan can be used to tune properties of Laponite cross-linked PEO nanocomposites for creating improved bioactive scaffolds for bone repair. Further development of these multiphase nanocomposite materials will include chemical mapping experiments of the nanocomposite surfaces to better understand how nanometer- and micrometer-sized heterogeneities influence cell adhesion and growth.

Acknowledgment. This research has been supported in part by an NSF CAREER award 0711783 to G.S., by a Purdue Lynn Doctoral fellowship to P.J.S., and in part by the Purdue Research Foundation.

REFERENCES AND NOTES

(1) Nettles, D. L.; Elder, S. H.; Gilbert, J. A. *Tissue Eng.* **2002**, *8*, 1009–1016.
(2) Kim, I.-Y.; Seo, S.-J.; Moon, H.-S.; Yoo, M.-K.; Park, I.-Y.; Kim, B.-C.; Cho, C.-S. *Biotechnol. Adv.* **2008**, *26*, 1–21.
(3) Di Martino, A.; Sittinger, M.; Risbud, M. V. *Biomaterials* **2005**, *26*, 5983–5990.
(4) Martins, A. M.; Alves, C. M.; Kasper, F. K.; Mikos, A. G.; Reis, R. L. *J. Mater. Chem.* **2010**, *20*, 1638–1645.
(5) Wei, C.-Z.; Hou, C.-L.; Gu, Q.-S.; Jiang, L.-X.; Zhu, B.; Sheng, A.-L. *Biomaterials* **2009**, *30*, 5534–5540.
(6) Tomihata, K.; Ikada, Y. *Biomaterials* **1997**, *18*, 567–575.
(7) Wu, Y.-C.; Shaw, S.-Y.; Lin, H.-R.; Lee, T.-M.; Yang, C.-Y. *Biomaterials* **2006**, *27*, 896–904.
(8) Chua, P.-H.; Neoh, K.-G.; Kang, E.-T.; Wang, W. *Biomaterials* **2008**, *29*, 1412–1421.
(9) Guzmán-Morales, J.; El-Gabalawy, H.; Pham, M. H.; Tran-Khanh, N.; McKee, M. D.; Wu, W.; Centola, M.; Hoemann, C. D. *Bone* **2009**, *45*, 617–626.
(10) Murakami, K.; Aoki, H.; Nakamura, S.; Nakamura, S.-i.; Takikawa, M.; Hanzawa, M.; Kishimoto, S.; Hattori, H.; Tanaka, Y.; Kiyosawa, T.; Sato, Y.; Ishihara, M. *Biomaterials* **2010**, *31*, 83–90.
(11) Jiao, H.; Yao, J.; Yang, Y.; Chen, X.; Lin, W.; Li, Y.; Gu, X.; Wang, X. *Biomaterials* **2009**, *30*, 5004–5018.
(12) Malafaya, P. B.; Reis, R. L. *Acta Biomater.* **2009**, *5*, 644–660.
(13) Tadanao, F.; Tokifumi, M.; Norimasa, I.; Shintaro, Y.; Tatsuya, M.; Akio, M.; Kazuo, H.; Hiroshi, T.; Seiichi, T.; Shin-Ichiro, N. *J. Biomed. Mater. Res., Part A* **2005**, *74A*, 338–346.
(14) Chen, R.-N.; Wang, G.-M.; Chen, C.-H.; Ho, H.-O.; Sheu, M.-T. *Biomacromolecules* **2006**, *7*, 1058–1064.
(15) Zhou, Y.; Yang, D.; Chen, X.; Xu, Q.; Lu, F.; Nie, J. *Biomacromolecules* **2007**, *9*, 349–354.
(16) Kuo, Y.-C.; Hsu, Y.-R. *J. Biomed. Mater. Res., Part A* **2008**, *91*, 277–87.
(17) Kuo, Y.-C.; Ku, I. N. *Biomacromolecules* **2008**, *9*, 2662–2669.
(18) Griffith, L. G.; Naughton, G. *Science* **2002**, *295*, 1009–1014.
(19) Ratner, B. D.; Bryant, S. J. *Annu. Rev. Biomed. Eng.* **2004**, *6*, 41–75.
(20) Jin, Q.; Schexnailder, P.; Gaharwar, A. K.; Schmidt, G. *Macromol. Biosci.* **2009**, *9*, 1028–1035.
(21) Gaharwar, A. K.; Schexnailder, P.; Kaul, V.; Akkus, O.; Zakharov, D.; Seifert, S.; Schmidt, G. *Adv. Funct. Mater.* **2010**, *20*, 429–436.
(22) Schexnailder, P. J.; Gaharwar, A. K.; Bartlett, R. L., II; Seal, B. L.; Schmidt, G. *Macromol. Biosci.* **2010**, *10*, DOI: 10.1002/mabi.201000053.
(23) Hench, L. L. *J. Eur. Ceram. Soc.* **2009**, *29*, 1257–1265.
(24) Kokubo, T. *Biomaterials* **1991**, *12*, 155–163.
(25) Larry, L. H. *J. Am. Ceram. Soc.* **1991**, *74*, 1487–1510.
(26) Blaker, J. J.; Gough, J. E.; Maquet, V.; Notingher, I.; Boccaccini, A. R. *J. Biomed. Mater. Res., Part A* **2003**, *67A*, 1401–1411.
(27) Couto, D. S.; Hong, Z.; Mano, J. F. *Acta Biomater.* **2009**, *5*, 115–123.
(28) Peter, M.; Binulal, N. S.; Nair, S. V.; Selvamurugan, N.; Tamura, H.; Jayakumar, R. *Chem. Eng. J.* **2010**, *158*, 353–361.
(29) Dundigalla, A.; Lin-Gibson, S.; Ferreiro, V.; Malwitz, M. M.; Schmidt, G. *Macromol. Rapid Commun.* **2005**, *26*, 143–149.
(30) Clapp, C. E.; Emerson, W. W. *Soil Sci.* **1972**, *114*, 210–216.
(31) Darder, M.; Colilla, M.; Ruiz-Hitzky, E. *Chem. Mater.* **2003**, *15*, 3774–3780.
(32) Darder, M.; Colilla, M.; Ruiz-Hitzky, E. *Appl. Clay Sci.* **2005**, *28*, 199–208.
(33) Zheng, J. P.; Wang, C. Z.; Wang, X. X.; Wang, H. Y.; Zhuang, H.; Yao, K. D. *React. Funct. Polym.* **2007**, *67*, 780–788.
(34) Zivanovic, S.; Li, J.; Davidson, P. M.; Kit, K. *Biomacromolecules* **2007**, *8*, 1505–1510.
(35) Kabiri, K.; Mirzadeh, H.; Zohuriaan-Mehr, M. J. *J. Appl. Polym. Sci.* **2010**, *116*, 2548–2556.
(36) Ritger, P. L.; Peppas, N. A. *J. Controlled Release* **1987**, *5*, 23–36.
(37) Kim, B.; Peppas, N. A. *Biomed. Microdevices* **2003**, *5*, 333–341.
(38) Guilherme, M. R.; Fajardo, A. R.; Moia, T. A.; Kunita, M. H.; Gonçalves, M. d. C.; Rubira, A. F.; Tambourgi, E. B. *Eur. Polym. J.* **2010**, *46*, 1465–1474.
(39) Depan, D.; Kumar, A. P.; Singh, R. P. *Acta Biomater.* **2009**, *5*, 93–100.
(40) Wu, C.-J.; Gaharwar, A. K.; Schexnailder, P. J.; Schmidt, G. *Materials* **2010**, *3*, 2986–3005.
(41) Porstmann, B.; Jung, K.; Schmechta, H.; Evers, U.; Pergande, M.; Porstmann, T.; Kramm, H.-J.; Krause, H. *Clin. Biochem.* **1989**, *22*, 349–355.
(42) Zhuang, H.; Zheng, J. P.; Gao, H.; De Yao, K. *J. Mater. Sci.: Mater. Med.* **2007**, *18*, 951–957.
(43) Niu, X.; Feng, Q.; Wang, M.; Guo, X.; Zheng, Q. *J. Controlled Release* **2009**, *134*, 111–117.
(44) Macosko, C. W. *Rheology: Principles, Measurements and Applications*; Wiley-VCH: New York, 1994.
(45) Cai, K.; Yao, K.; Cui, Y.; Lin, S.; Yang, Z.; Li, X.; Xie, H.; Qing, T.; Luo, J. *J. Biomed. Mater. Res., Part A* **2002**, *60*, 398–404.
(46) Anselme, K. *Biomaterials* **2000**, *21*, 667–681.
(47) Mammoto, A.; Ingber, D. E. *Curr. Opin. Cell Biol.* **2009**, *21*, 864–870.
(48) Rawadi, G.; Vayssiere, B.; Dunn, F.; Baron, R.; Roman-Roman, S. *J. Bone Miner. Res.* **2003**, *18*, 1842–1853.
(49) Wang, D.; Christensen, K.; Chawla, K.; Xiao, G.; Krebsbach, P. H.; Franceschi, R. T. *J. Bone Miner. Res.* **1999**, *14*, 893–903.
(50) Moreau, J. L.; Xu, H. H. K. *Biomaterials* **2009**, *30*, 2675–2682.
(51) Coutinho, D. F.; Pashkuleva, I. H.; Alves, C. M.; Marques, A. P.; Neves, N. M.; Reis, R. L. *Biomacromolecules* **2008**, *9*, 1139–1145.
(52) Malaval, L.; Liu, F.; Roche, P.; Aubin, J. E. *J. Cell. Biochem.* **1999**, *74*, 616–627.
(53) Sudo, H.; Kodama, H. A.; Amagai, Y.; Yamamoto, S.; Kasai, S. *J. Cell Biol.* **1983**, *96*, 191–198.
(54) Weir, M. D.; Xu, H. H. K. *J. Biomed. Mater. Res., Part A* **2010**, *94A*, 223–233.
(55) Yang, X.; Chen, X.; Wang, H. *Biomacromolecules* **2009**, *10*, 2772–2778.

AM100609T